A Modelling and simulation of a sensorless control of five-phase PMSM drives using multi-dimension space vector modulation

Kamel Saleh, Mark Sumner

An-Najah National University Palestine, University of Nottingham UK.
E-Mail: kamel.saleh@najah.edu

Abstract

This paper introduces a new method to track the saturation saliency for position measurement of a five-phase PMSM motor fed by a five-phase inverter through measuring the dynamic current response of the motor line currents due to the IGBT switching actions. The new method uses only the fundamental PWM waveform obtained using the multi-phase space vector pulse width modulation (i.e there is no modification to the operation of the five-phase inverter) similar to the fundamental PWM method proposed for a three-leg inverter. Simulation results are provided to verify the effectiveness of the proposed strategy for saliency tracking of a five-phase PMSM motor driven by five-phase inverter over a wide speed ranges under different load conditions.

Keywords*: Sensorless, five-phase motor, multi-dimension SVPWM.*

1. Introduction

The interest in multi-phase motor drives has increased in recent years as they offer several advantages when compared to three-phase machines such as[1, 2]:-

1) Improved reliability and increased fault tolerance;
2) Greater efficiency;
3) Higher torque density and reduced torque pulsations;

Therefore, multi-phase motor drives are extensively considered for applications related to vehicles, aerospace application (more electric craft), ship propulsion and high power applications.

As multi-phase motor drives are multi-dimensional systems and since most multi-phase motors are designed to have a non-sinusoidal back EMF, therefore conventional PWM which is implemented only in two-dimensional d-q subspace and aims to realize a sinusoidal phase voltage is no longer suitable. Instead multi-phase PWM techniques are of key important and have been the subject much research. SVPWM strategy is presented based on the concept of orthogonal multi-dimensional vector space in [3, 4, 5, 6, 7, 8, 9, 10, 11, 12], which can synthesize voltage vectors both in d-q subspace and in other subspaces to satisfy motor control requirements.

Tracking the saliency of ac motors fed by two level three-leg inverters has been widely researched. At low and zero speed, some form of additional excitation has been proposed, such as the injection of a high frequency (HF) voltage or current [13, 14, 15] or the injection of test pulses [16, 17, 18].

Many control techniques has been adopted to control the multi-phase motor drives in sensored mode such as Fuzzy Logic Control [19], predictive current control [20]. In the last couple of years, few researches have been directed towards the sensorless control of a multi-phase electrical drives. These researches focus on the model based sensorless control, direct torque control and high frequency injections[21, 22, 23, 24, 25].

This paper proposes a new method to track saliency in a five phase inverter PMSM drive for example to track the saturation saliency in five PM motors and rotor slotting saliency in five-phase induction motors without introducing any modification to the operation of the drive system. It simply measures the transient response of the phases currents when active and switching zero vectors are applied.

2. Research Method

2.1 Five-phase converter drive topology

Figure 1 shows the proposed five-phase converter drive topology [23]. The motor model is given by (1) to (5).

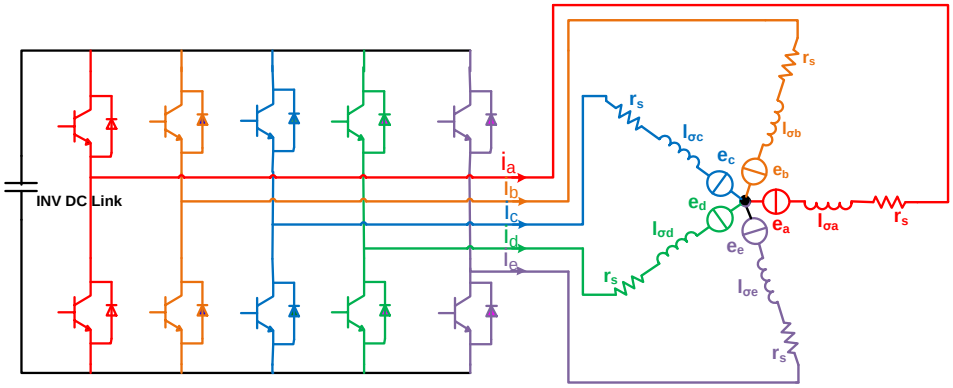

Figure 1. Five phase converter drive topology.

$v_a = r_s \times i_a + \frac{d\varphi_a}{dt}$ ..... (1) , $v_b = r_s \times i_b + \frac{d\varphi_b}{dt}$ ..... (2) , $v_c = r_s \times i_c + \frac{d\varphi_c}{dt}$ ..... (3)

$v_d = r_s \times i_d + \frac{d\varphi_d}{dt}$ ..... (4) , $v_e = r_s \times i_e + \frac{d\varphi_e}{dt}$ ..... (5)

Where v_a, v_b, v_c, v_d, v_e are the external voltages applied to the motor, r_s the equivalent resistance of the stator phase winding, i_a, i_b, i_c, i_d, i_e are the stator phase currents , $\frac{d\varphi_a}{dt}$, $\frac{d\varphi_b}{dt}$, $\frac{d\varphi_c}{dt}$, $\frac{d\varphi_d}{dt}$, $\frac{d\varphi_e}{dt}$ are the rate of changes of the magnetic flux in the phases. The permanent magnet and the five windings contribute to the total flux linking each winding as given:-

$\varphi_a = L_{aa} \times i_a + L_{ab} \times i_b + L_{ac} \times i_c + L_{ad} \times i_d + L_{ae} \times i_e + \varphi_{ma}$ ..... (6)

$\varphi_b = L_{ab} \times i_a + L_{bb} \times i_b + L_{bc} \times i_c + L_{bd} \times i_d + L_{be} \times i_e + \varphi_{mb}$ ..... (7)

$\varphi_c = L_{ac} \times i_a + L_{bc} \times i_b + L_{cc} \times i_c + L_{cd} \times i_d + L_{ce} \times i_e + \varphi_{mc}$ ..... (8)

$\varphi_d = L_{ad} \times i_a + L_{bd} \times i_b + L_{cd} \times i_c + L_{dd} \times i_d + L_{de} \times i_e + \varphi_{md}$ ..... (9)

$\varphi_e = L_{ae} \times i_a + L_{be} \times i_b + L_{ce} \times i_c + L_{de} \times i_d + L_{ee} \times i_e + \varphi_{me}$ ..... (10)

where: φ_a, φ_b, φ_c, φ_d and φ_e are the total fluxes linking each stator winding.

L_{aa}, L_{bb}, L_{cc}, L_{dd} and L_{ee} are the self-inductances of the stator windings.

L_{ab}, L_{ac} , L_{ba} ,L_{ad}, L_{ae}, L_{bc} , L_{bd} , L_{be} , L_{cd} , L_{ce} and L_{de} are the mutual inductances of the stator windings.

φ_{ma}, φ_{mb}, φ_{mc} , φ_{md}, and φ_{me} are the permanent magnet fluxes linking the stator windings.

The inductances in the stator windings are functions of rotor angle, defined by

$L_{aa} = L_{so} + L_{sl} + L_x cos(2\theta)$ ..... (11), $L_{bb} = L_{so} + L_{sl} + L_x cos(2\theta - 72^\circ)$ .... (12)

$L_{cc} = L_{so} + L_{sl} + L_x cos(2\theta - 144^\circ)$ ..... (13), $L_{dd} = L_{so} + L_{sl} + L_x cos(2\theta - 216^\circ)$ ..... (14)

$L_{ee} = L_{so} + L_{sl} + L_x \cos(2\theta - 288^\circ)$ ... (15),

$L_{ab} = L_{ba} = L_{so}\cos(72^\circ) + L_x cos(2\theta - 72^\circ)$ ... (16) ,

$L_{ac} = L_{ca} = L_{so}\cos(144^\circ) + L_x cos(2\theta - 144^\circ)$ ...(17)

$L_{ad} = L_{da} = L_{so}\cos(216^\circ) + L_x cos(2\theta - 216^\circ)$ .... (18)

$L_{ae} = L_{ea} = L_{so}\cos(288^\circ) + L_x cos(2\theta + 288^\circ)$ ... (19),

$L_{bc} = L_{cb} = L_{so}\cos(72^\circ) + L_x cos(2\theta - 216^\circ)$ .... (20)

$L_{bd} = L_{db} = L_{so}\cos(144^\circ) + L_x cos(2\theta - 288^\circ)$ ... (21)

$L_{be} = L_{eb} = L_{so}\cos(144^\circ) + L_x cos(2\theta)$ ..... (22)

$L_{cd} = L_{dc} = L_{so}\cos(72^\circ) + L_x cos(2\theta)$ ..... (23),

$L_{ce} = L_{ec} = L_{so}\cos(144^\circ) + L_x cos(2\theta - 72^\circ)$ ..... (24)

$L_{de} = L_{ed} = L_{so}\cos(72^\circ) + L_x cos(2\theta - 144)$ ..... (25)

where: L_{sl} is the stator self-inductance per phase. This is the average self-inductance of each of the stator windings. L_x is the stator inductance fluctuation. L_{so} is the stator mutual inductance. This is the average

mutual inductance between the stator windings. The effects of saturation saliency appeared in stator self and mutual inductances are indicated by the term (2θ).
The flux-linkages at the stator windings due to the permanent magnet are:
$\varphi_{ma} = \lambda_m \times cos(\theta)$ (26) , $\varphi_{mb} = \lambda_m \times cos(\theta - 72^{\circ})$ (27) , $\varphi_{mc} = \lambda_m \times cos(\theta - 144^{\circ})$ (28)
$\varphi_{md} = \lambda_m \times cos(\theta - 216)$ ……..(29) , $\varphi_{me} = \lambda_m \times cos(\theta - 288^{\circ})$ …….(30)
Where φ_m is the peak flux linkage due to permanent magnet.

2.2 Multi-phase Space Vector Pulse Width Modulation

2.2.1 Concept of Orthogonal Vector Space

The difference between the space vector modulation of the five-phase motors and those proposed for a three-phase motors is that the kth order harmonics (k = 5×m ± 2, m = 1,3,5...) of the machine's variables such as phase voltage, phase current which do not produce any rotating MMF and are non electromechanical energy conversion related will freely flow through the machine and their amplitude will be restricted by the stator leakage impedance only [3-12 ,21-25]. Hence, generation of certain low-order voltage harmonics (3rd harmonic) in the VSI output can lead to large 3rd harmonic in stator current . It is therefore important that the multi-phase VSI output is kept as close as possible to sinusoidal. To do so the reference voltage should be mapped into two orthogonal planes. The first one is the d1-q1 plane that is rotating at synchronous speed and has fundamental components of the reference voltage. The second is the d3-q3 plane that is rotating at 3 times the synchronous speed and has the 3rd harmonic components of the reference voltage using the transformation given in (31) and (32):-

$$\begin{bmatrix} d1 \\ q1 \\ d3 \\ q3 \end{bmatrix} = [G] \begin{bmatrix} a \\ b \\ c \\ d \\ e \end{bmatrix} \ldots \text{(31)} \quad \text{and} \quad \begin{bmatrix} a \\ b \\ c \\ d \\ e \end{bmatrix} = [G^{-1}] \begin{bmatrix} d1 \\ q1 \\ d3 \\ q3 \end{bmatrix} \ldots \text{(32)}$$

Where

$$G = \frac{2}{5} \begin{bmatrix} \sin(\theta) & \sin(\theta - 72^{\circ}) & \sin(\theta - 144^{\circ}) & \sin(\theta - 216^{\circ}) & \sin(\theta - 288^{\circ}) \\ \cos(\theta) & \cos(\theta - 72^{\circ}) & \cos(\theta - 144^{\circ}) & \cos(\theta - 216^{\circ}) & \cos(\theta - 288^{\circ}) \\ \sin(3\theta) & \sin(3(\theta - 72^{\circ})) & \sin(3(\theta - 144^{\circ})) & \sin(3(\theta - 216^{\circ})) & \sin(3(\theta - 288^{\circ})) \\ \cos(3\theta) & \cos(3(\theta - 72^{\circ})) & \cos(3(\theta - 144^{\circ})) & \cos(3(\theta - 216^{\circ})) & \cos(3(\theta - 288^{\circ})) \end{bmatrix} \text{(33)}$$

Using equations 31 and 32 are very important as the fundamental and the third harmonics of the five-phase variables can be regarded as dc components making thier control is easy. In the other hand, the choosing of the switching voltages and the calculation of the application times of the switching vectors need to map the fundamental and the third harmonics of the five-phase variables to a two orthogonal stationary frames α1-β1 and α3-β3 according to (34,35,36). The

$$\begin{bmatrix} \alpha 1 \\ \beta 1 \\ \alpha 3 \\ \beta 3 \end{bmatrix} = [H] \begin{bmatrix} a \\ b \\ c \\ d \\ e \end{bmatrix} \ldots\ldots\ldots \text{(34)} \quad \text{And} \quad \begin{bmatrix} a \\ b \\ c \\ d \\ e \end{bmatrix} = [H^{-1}] \begin{bmatrix} \alpha 1 \\ \beta 1 \\ \alpha 3 \\ \beta 3 \end{bmatrix} \ldots\ldots \text{(35)} \text{ , Where}$$

$$H = \frac{2}{5} \begin{bmatrix} 1 & \cos(72^{\circ}) & \cos(144^{\circ}) & \cos(216^{\circ}) & \cos(288^{\circ}) \\ 0 & \sin(72^{\circ}) & \sin(144^{\circ}) & \sin(216^{\circ}) & \sin(288^{\circ}) \\ 1 & \cos(216^{\circ}) & \cos(72^{\circ}) & \cos(288^{\circ}) & \cos(144^{\circ}) \\ 0 & \sin(216^{\circ}) & \sin(72^{\circ}) & \sin(288^{\circ}) & \sin(144^{\circ}) \end{bmatrix} \ldots\ldots\ldots\ldots\ldots \text{(36)}$$

Using the equation (34 ,35,36) there are 32 space vectors, two of which are zero vectors(00000 and 11111). Thirty non-zero space voltage vectors of a five-phase inverter can be projected to α1-β1 plane and α3-β3 palne as shown in Figure 2. In α1-β1 palne, the thirty vectors are composed of three sets of different amplitude vectors, and divide α1-β1 plane into 10 sectors. The amplitudes of these voltage vectors are [3-12, 21]:-
Vmin = 0.2472Vdc, (11001), (11000), (11100), (01100), (01110), (00110), (00111), (00011), (10011), (10001).
Vmid = 0.4Vdc, (10000), (11101), (01000), (11110), (00100),(01111), (00010), (10111), (00001), (11011).
Vmax = 0.6472Vdc, (01001), (11010), (10100), (01101), (01010), (10110), (00101), (01011), (10010), (10101). And the ratio of the amplitudes is 1:1.618:1.6182. It is the same situation in the α3-β3 plane.

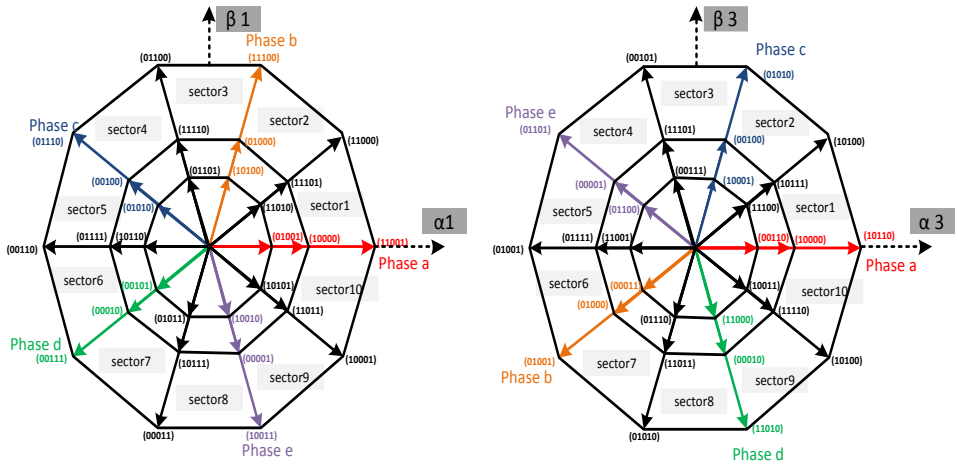

Figure 2. Thirty nonzero switching vectors on α1 –β1 plane and α3 –β3 plane.

From the average vector concept during one sampling period [12], a reference voltage vector on the α1-β1 plane can be realized by adjusting the application times of the nearest two Vmid switching vectors and two Vmax switching vectors. The other combinations of switching vectors increase the number of switching or decrease the maximum magnitude of the realizable voltage vector.

2.2.2 Calculation of the Application Times for the Switching Vectors

Figure 3 shows the reference voltage of the fundamental component (Vref_ α1-β1) exists in the first quadrant in the α1-β1 plane and the third harmonic component of the reference voltage (Vref_ α3-β3) located in the first sector in the α3-β3 plan. For both reference voltages, the vectors (00000, 10000, 11000, 01001, 11101, 11111) are used to utilize them in both α1-β1 and α3-β3 planes as shown in figure 3.

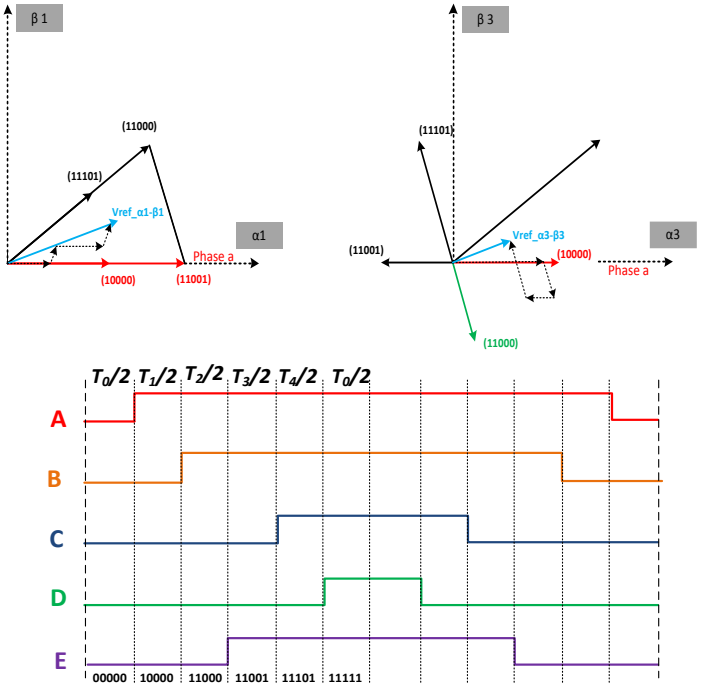

Figure 3. Realization of a reference voltage vector located in sector 1 on the d –q plane and the associated switching sequence

The time needed for applying each vectors can be calculated as:-

$$\begin{bmatrix} T_1 \\ T_2 \\ T_3 \\ T_4 \end{bmatrix} = Ts \times [T^{-1}] \begin{bmatrix} \text{Vref\_}\alpha 1 \\ \text{Vref\_}\beta 1 \\ \text{Vref\_}\alpha 3 \\ \text{Vref\_}\beta 3 \end{bmatrix} \quad \ldots\ldots \quad (37)$$ Where

$$\text{T} = \begin{bmatrix} V_{mid} & V_{max}\cos(72^{\circ}) & V_{max} & V_{mid}\cos(72^{\circ}) \\ 0 & V_{max}\sin(72^{\circ}) & 0 & V_{mid}\sin(72^{\circ}) \\ V_{mid} & V_{min}\cos(288^{\circ}) & -V_{min} & V_{mid}\cos(108^{\circ}) \\ 0 & V_{min}\sin(288^{\circ}) & 0 & V_{mid}\sin(108^{\circ}) \end{bmatrix} \quad \ldots\ldots\ldots\ldots\ldots \quad (38)$$

$$T_0 = T_s - T_1 - T_2 - T_3 - T_4 \quad \ldots\ldots\ldots\ldots\ldots \quad (39)$$

The same approach can be applied for other sectors.

2.3 Sensored Operation of the Five-phase Drive

Figure 4 shows the vector control structure proposed for the five-phase drive system when using an encoder for feedback i.e in sensored mode. It can be seen that the third harmonic component is controlled to be zero through putting id3_ref and iq3_ref to zero.

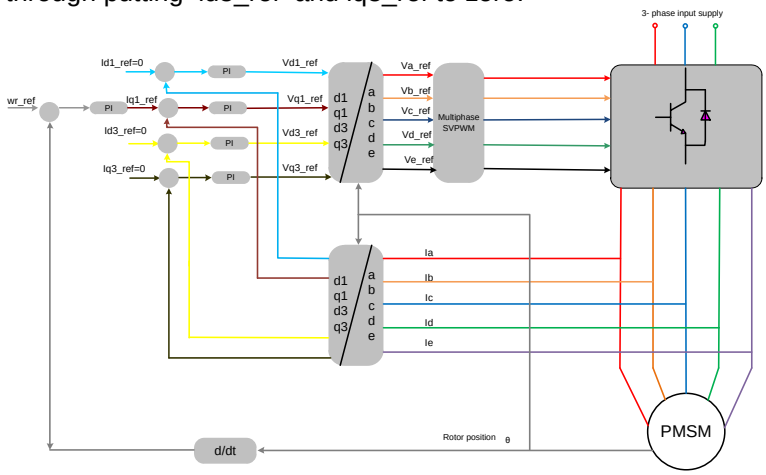

Figure 4. Vector control topology using multi dimensions space vector PWM for five -phase drive

The simulation of the five-phase converter PMSM drive has been carried out using the SABER simulation package. Figure 5 shows the feasibility of the system. At 0.2 s a speed step of 100 rpm is applied to the drive then at t = 0.9 s a load step is applied to the system. In both cases the system drive could recover in short time period.

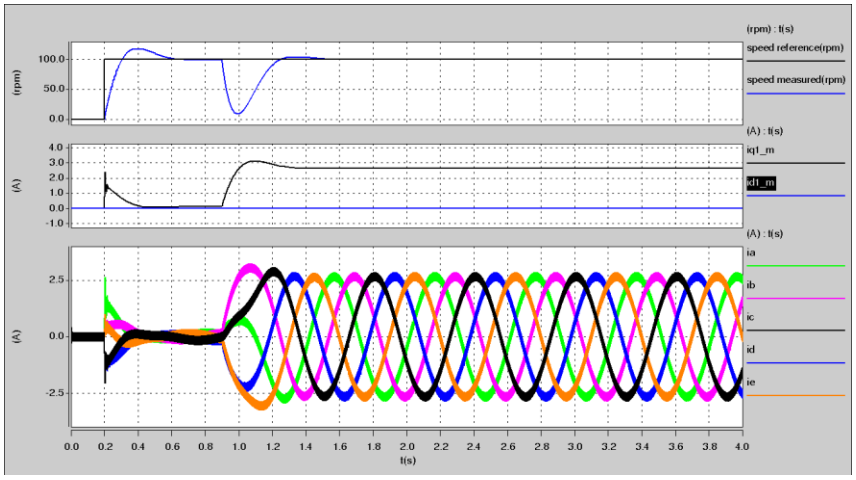

Figure 5. Sensored operation of the five phase motor

FFT was carried out on the current waveform in time interval between 2 s and 4 s (steady state) to show if there is a third harmonic component in the current or not and the result is given in figure 6. As can be seen from figure 6, the current spectrum only has the fundamental frequency only and the third harmonic does not exist in the current spectrum as its reference values (id3_ref and iq3_ref) are put equal zero.

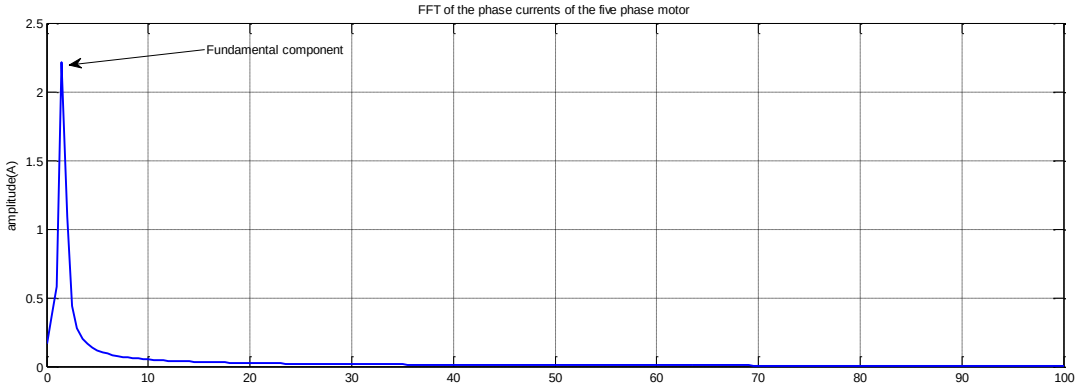

Figure 6. FFT of the phase currents of the five phase drive under speed control

2.4 Algorithm for tracking the saturation saliency of five phase PMSM

The stator windings self-inductances are modulated by the anisotropy obtained by the saturation saliency of main flux and this can be expressed as[23]:-

$l\sigma a = L_{so} + L_{sl} + L_x cos(2\theta)$ …… (40) , $l\sigma b = L_{so} + L_{sl} + L_x cos(2\theta - 72^{\circ})$ …. (41)

$l\sigma c = L_{so} + L_{sl} + L_x cos(2\theta - 144^{\circ})$ … (42) , $l\sigma d = L_{so} + L_{sl} + L_x cos(2\theta - 216^{\circ})$ … (43)

$l\sigma e = L_{so} + L_{sl} + L_x cos(2\theta - 288^{\circ})$ … (44)

This modulation will be reflected in the transient response of the motor line current to the test vector imposed by the inverter. So by using the fundamental PWM wave form and by measuring the transient current response to the active vectors it is possible to detect the inductance variation and track the rotor position Figure 7 shows the space vector modulation state diagram for a five-phase inverter when V_ref_α1-β1 exists in first sector. The switching sequences and the timing of the applied vectors will be :-

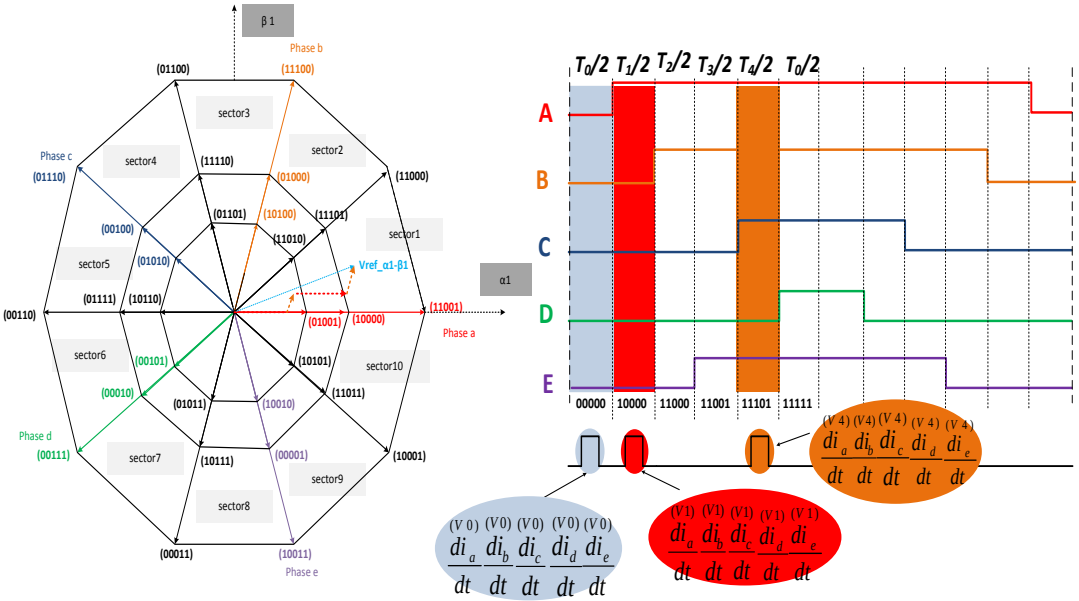

Figure 7. Space vector modulation state diagram for five phase inverter in case that V_ref_α1-β1 exists in first sector

The stator circuit when the vectors V1,V4 and V0 are applied are shown in Figure 8.a, figure 8.b and figure 8.c respectively.

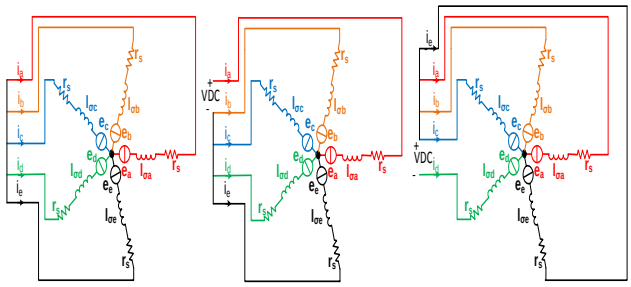

Figure 8. Stator circuits when: (a) V1 is applied; (b) V2 is applied; (c) V0 is applied

Using the circuit in Figure 8.a, the following equations hold true:-

$$0 = r_s * i_a{}^{(V0)} + l_{\sigma a} * \frac{di_a^{(V0)}}{dt} + e_a^{(V0)} - r_s * i_b{}^{(V0)} - l_{\sigma b} * \frac{di_b^{(V0)}}{dt} - e_b^{(V0)} \quad \text{..... (45)}$$

$$0 = r_s * i_b{}^{(V0)} + l_{\sigma b} * \frac{di_b^{(V0)}}{dt} + e_b^{(V0)} - r_s * i_c{}^{(V0)} - l_{\sigma c} * \frac{di_c^{(V0)}}{dt} - e_c^{(V0)} \quad \text{..... (46)}$$

$$0 = r_s * i_c{}^{(V0)} + l_{\sigma c} * \frac{di_c^{(V0)}}{dt} + e_c^{(V0)} - r_s * i_d{}^{(V0)} - l_{\sigma d} * \frac{di_d^{(V0)}}{dt} - e_d^{(V0)} \quad \text{..... (47)}$$

$$0 = r_s * i_d{}^{(V0)} + l_{\sigma d} * \frac{di_d^{(V0)}}{dt} + e_d^{(V0)} - r_s * i_e{}^{(V0)} - l_{\sigma e} * \frac{di_e^{(V0)}}{dt} - e_e^{(V0)} \quad \text{..... (48)}$$

$$0 = r_s * i_e{}^{(V0)} + l_{\sigma e} * \frac{di_e^{(V0)}}{dt} + e_e^{(V0)} - r_s * i_a{}^{(V0)} - l_{\sigma a} * \frac{di_a^{(V0)}}{dt} - e_a^{(V0)} \quad \text{..... (49)}$$

The following equations are obtained using Figure 8.b:-

$$V_{DC} = r_s * i_a{}^{(V1)} + l_{\sigma a} * \frac{di_a^{(V1)}}{dt} + e_a^{(V1)} - r_s * i_b{}^{(V1)} - l_{\sigma b} * \frac{di_b^{(V1)}}{dt} - e_b^{(V1)} \quad \text{.. (50)}$$

$$0 = r_s * i_b{}^{(V1)} + l_{\sigma b} * \frac{di_b^{(V0)}}{dt} + e_b^{(V1)} - r_s * i_c{}^{(V1)} - l_{\sigma c} * \frac{di_c^{(V1)}}{dt} - e_c^{(V1)} \quad \text{..... (51)}$$

$$0 = r_s * i_c{}^{(V1)} + l_{\sigma c} * \frac{di_c^{(V0)}}{dt} + e_c^{(V1)} - r_s * i_d{}^{(V1)} - l_{\sigma d} * \frac{di_d^{(V1)}}{dt} - e_d^{(V1)} \quad \text{..... (52)}$$

$$0 = r_s * i_d{}^{(V1)} + l_{\sigma d} * \frac{di_d^{(V0)}}{dt} + e_d^{(V1)} - r_s * i_e{}^{(V1)} + l_{\sigma e} * \frac{di_e^{(V1)}}{dt} - e_e^{(V1)} \quad \text{..... (53)}$$

$$-V_{DC} = r_s * i_e{}^{(V1)} + l_{\sigma e} * \frac{di_e^{(V0)}}{dt} + e_e^{(V1)} - r_s * i_a{}^{(V1)} - l_{\sigma a} * \frac{di_a^{(V1)}}{dt} - e_a^{(V1)} \quad \text{... (54)}$$

Finally when V0 is applied as shown in Figure 8.c, the following equations hold true:-

$$0 = r_s * i_a{}^{(V4)} + l_{\sigma a} * \frac{di_a^{(V4)}}{dt} + e_a^{(V4)} - r_s * i_b{}^{(V4)} - l_{\sigma b} * \frac{di_b^{(V4)}}{dt} - e_b^{(V4)} \quad \text{.....(55)}$$

$$0 = r_s * i_b{}^{(V4)} + l_{\sigma b} * \frac{di_b^{(V4)}}{dt} + e_b^{(V4)} - r_s * i_c{}^{(V4)} - l_{\sigma c} * \frac{di_c^{(V4)}}{dt} - e_c^{(V4)} \quad \text{..... (56)}$$

$$V_{DC} = r_s * i_c{}^{(V4)} + l_{\sigma c} * \frac{di_c^{(V4)}}{dt} + e_c^{(V4)} - r_s * i_d{}^{(V4)} - l_{\sigma d} * \frac{di_d^{(V4)}}{dt} - e_d^{(V4)} \quad \text{.....(57)}$$

$$-V_{DC} = r_s * i_d{}^{(V4)} + l_{\sigma d} * \frac{di_d^{(V4)}}{dt} + e_d^{(V4)} - r_s * i_e{}^{(V4)} - l_{\sigma e} * \frac{di_e^{(V4)}}{dt} - e_e^{(V4)} \quad \text{...(58)}$$

$$0 = r_s * i_e{}^{(V0)} + l_{\sigma e} * \frac{di_e^{(V4)}}{dt} + e_e^{(V4)} - r_s * i_a{}^{(V4)} - l_{\sigma a} * \frac{di_a^{(V4)}}{dt} - e_a^{(V4)} \quad \text{..... (59)}$$

Assuming that the voltage drop across the stator resistances are small and can be neglected and the back emf can be cancelled if the time separation between the vectors is small, these equations can be simplified as:-

$$\left(\frac{di_b^{(V1)}}{dt} - \frac{di_b^{(V0)}}{dt}\right) = C1 + C2 * \cos(2\theta - 216^\circ) \quad \text{(60)}, \quad \left(\frac{di_e^{(V1)}}{dt} - \frac{di_e^{(V0)}}{dt}\right) = C1 + C2 * \cos(2\theta - 144^\circ) \quad \text{(61)}$$

$$\left(\frac{di_c^{(V1)}}{dt} - \frac{di_c^{(V0)}}{dt}\right) = C1 + C3 * \cos(2\theta - 72^\circ) \text{ (62)}, \left(\frac{di_d^{(V1)}}{dt} - \frac{di_d^{(V0)}}{dt}\right) = C1 + C4 * \cos(2\theta - 288^\circ) \text{ (63)}$$

$$\left(\frac{di_a^{(V1)}}{dt} - \frac{di_a^{(V0)}}{dt}\right) = C4 + C5 * \cos(2\theta) \text{ (64)} \quad , \quad -\left(\frac{di_b^{(V4)}}{dt} - \frac{di_b^{(V0)}}{dt}\right) = C1 + C3 * \cos(2\theta - 144^\circ). \quad \text{(65)}$$

$$-\left(\frac{di_a^{(V4)}}{dt} - \frac{di_a^{(V0)}}{dt}\right) = C1 + C3 * \cos(2\theta - 288^\circ) \quad \text{(66)} \, , -\left(\frac{di_c^{(V4)}}{dt} - \frac{di_c^{(V0)}}{dt}\right) = C1 + C2 * \cos(2\theta) \, . \, \text{(67)}$$

$-\left(\frac{di_e^{(V4)}}{dt}-\frac{di_e^{(V0)}}{dt}\right)=C1+C2*\cos(2\theta-72^{\circ})$(68),$-\left(\frac{di_d^{(V4)}}{dt}-\frac{di_d^{(V0)}}{dt}\right)=C4+C5*\cos(2\theta-216^{\circ})$ (69)

Where:-

$C1=\frac{-V_{DC}*(L_{so}+L_{sl})^3}{5((L_{so}+L_{sl})^4+\frac{3}{4}*(L_{so}+L_{sl})^2*{L_x}^2+0.0506)}$… (70) , $C2=\frac{-V_{DC}*1.618*(L_{so}+L_{sl})^2*L_x}{5((L_{so}+L_{sl})^4+\frac{3}{4}*(L_{so}+L_{sl})^2*{L_x}^2+0.0506)}$….. (71)

$C3=\frac{V_{DC}*0.618*(L_{so}+L_{sl})^2*L_x}{5((L_{so}+L_{sl})^4+\frac{3}{4}*(L_{so}+L_{sl})^2*{L_x}^2+0.0506)}$….. (72) , $C4=\frac{V_{DC}*4*(L_{so}+L_{sl})^3}{5((L_{so}+L_{sl})^4+\frac{3}{4}*(L_{so}+L_{sl})^2*{L_x}^2+0.0506)}$….. (73)

$C5=\frac{-V_{DC}*3*(L_{so}+L_{sl})^2*L_x}{5\left((L_{so}+L_{sl})^4+\frac{3}{4}*(L_{so}+L_{sl})^2*{L_x}^2+0.0506\right)}$….. (74) ,

It can be seen form equations above that transient response of the stator phase currents provides information about the saliency position and hence the rotor position. It should be mentioned here that each transient response will give a different offset and scale. Therefor, the construction of position scalars Pa, Pb,Pc,Pd and Pe are chosen among equations above to have the same offset as shown in table1 .

The postion scalars Pa, Pb,Pc,Pd and Pe can be transformed into P_α , P_β and can then be used to denote the orientation angle as follows :-

$\begin{bmatrix}P_\alpha\\P_\beta\end{bmatrix}=[V]\begin{bmatrix}a\\b\\c\\d\\e\end{bmatrix}\left(\frac{di_d^{(V4)}}{dt}-\frac{di_d^{(V0)}}{dt}\right)$ …….. (75) , Where

$V=\begin{bmatrix}1 & \cos(216^{\circ}) & \cos(72^{\circ}) & \cos(288^{\circ}) & \cos(144^{\circ})\\0 & \sin(216^{\circ}) & \sin(72^{\circ}) & \sin(288) & \sin(144^{\circ})\end{bmatrix}$….. (76)

Table Selection of pa, pb and pc for a star-connected five machine

Sector no	P_a	P_b	P_c	P_d	P_e
1	$\frac{di_c^{(V0)}}{dt}-\frac{di_c^{(V4)}}{dt}$	$\frac{di_e^{(V0)}}{dt}-\frac{di_e^{(V4)}}{dt}$	$\frac{di_e^{(V1)}}{dt}-\frac{di_e^{(V0)}}{dt}$	$\frac{di_b^{(V1)}}{dt}-\frac{di_b^{(V0)}}{dt}$	-(P_a +P_b +P_c +P_d)
2	$\frac{di_c^{(V0)}}{dt}-\frac{di_c^{(V4)}}{dt}$	$\frac{di_e^{(V0)}}{dt}-\frac{di_e^{(V4)}}{dt}$	-(P_a +P_b +P_d +P_e)	$\frac{di_a^{(V1)}}{dt}-\frac{di_a^{(V0)}}{dt}$	$\frac{di_c^{(V1)}}{dt}-\frac{di_{ac}^{(V0)}}{dt}$
3	-(P_b +P_c +P_d +P_e)	$\frac{di_d^{(V0)}}{dt}-\frac{di_d^{(V4)}}{dt}$	$\frac{di_a^{(V0)}}{dt}-\frac{di_a^{(V4)}}{dt}$	$\frac{di_a^{(V1)}}{dt}-\frac{di_a^{(V0)}}{dt}$	$\frac{di_c^{(V1)}}{dt}-\frac{di_c^{(V0)}}{dt}$
4	$\frac{di_d^{(V1)}}{dt}-\frac{di_d^{(V0)}}{dt}$	$\frac{di_d^{(V0)}}{dt}-\frac{di_d^{(V4)}}{dt}$	$\frac{di_a^{(V0)}}{dt}-\frac{di_a^{(V4)}}{dt}$	-(Pa +Pb+Pc+Pe)	$\frac{di_b^{(V1)}}{dt}-\frac{di_{ab}^{(V0)}}{dt}$
5	$\frac{di_d^{(V1)}}{dt}-\frac{di_d^{(V0)}}{dt}$	-(P_a +P_c+P_d+P_e)	$\frac{di_e^{(V0)}}{dt}-\frac{di_e^{(V4)}}{dt}$	$\frac{di_b^{(V0)}}{dt}-\frac{di_b^{(V4)}}{dt}$	$\frac{di_b^{(V1)}}{dt}-\frac{di_{ab}^{(V0)}}{dt}$
6	$\frac{di_c^{(V1)}}{dt}-\frac{di_c^{(V0)}}{dt}$	$\frac{di_e^{(V1)}}{dt}-\frac{di_e^{(V0)}}{dt}$	$\frac{di_e^{(V0)}}{dt}-\frac{di_e^{(V4)}}{dt}$	$\frac{di_b^{(V0)}}{dt}-\frac{di_b^{(V4)}}{dt}$	-(P_a +P_b+P_c+P_d)
7	$\frac{di_c^{(V1)}}{dt}-\frac{di_c^{(V0)}}{dt}$	$\frac{di_e^{(V1)}}{dt}-\frac{di_e^{(V0)}}{dt}$	-(P_a +P_b+P_d+P_e)	$\frac{di_a^{(V0)}}{dt}-\frac{di_a^{(V4)}}{dt}$	$\frac{di_c^{(V0)}}{dt}-\frac{di_c^{(V4)}}{dt}$
8	-(P_b +P_c+P_d+P_e)	$\frac{di_d^{(V1)}}{dt}-\frac{di_d^{(V0)}}{dt}$	$\frac{di_a^{(V1)}}{dt}-\frac{di_a^{(V0)}}{dt}$	$\frac{di_a^{(V0)}}{dt}-\frac{di_a^{(V4)}}{dt}$	$\frac{di_c^{(V0)}}{dt}-\frac{di_c^{(V4)}}{dt}$
9	$\frac{di_d^{(V0)}}{dt}-\frac{di_d^{(V4)}}{dt}$	$\frac{di_d^{(V1)}}{dt}-\frac{di_d^{(V0)}}{dt}$	$\frac{di_a^{(V1)}}{dt}-\frac{di_a^{(V0)}}{dt}$	-(P_a +P_b+P_c+P_e)	$\frac{di_b^{(V0)}}{dt}-\frac{di_b^{(V4)}}{dt}$
10	$\frac{di_d^{(V0)}}{dt}-\frac{di_d^{(V4)}}{dt}$	-(Pa +Pc+Pd+Pe)	$\frac{di_e^{(V1)}}{dt}-\frac{di_e^{(V0)}}{dt}$	$\frac{di_b^{(V1)}}{dt}-\frac{di_b^{(V0)}}{dt}$	$\frac{di_b^{(V0)}}{dt}-\frac{di_b^{(V4)}}{dt}$

3. Results and Analysis

3.1 Position and Speed Estimation Under Sensored Operation

The validation of the saliency tracking algorithm given in table 1 is made using the vector control structure working in sensored mode shown in figure 9 . The mechanical observer [13] is used to filter out the high frequency noise in the position signals. The whole vector control structure has been implemented in simulation in the Saber modeling environment. Note the simulation includes a minimum pulsewidth of 10us when di/dt measurements are made – a realistic values seen from experimental results of [18].

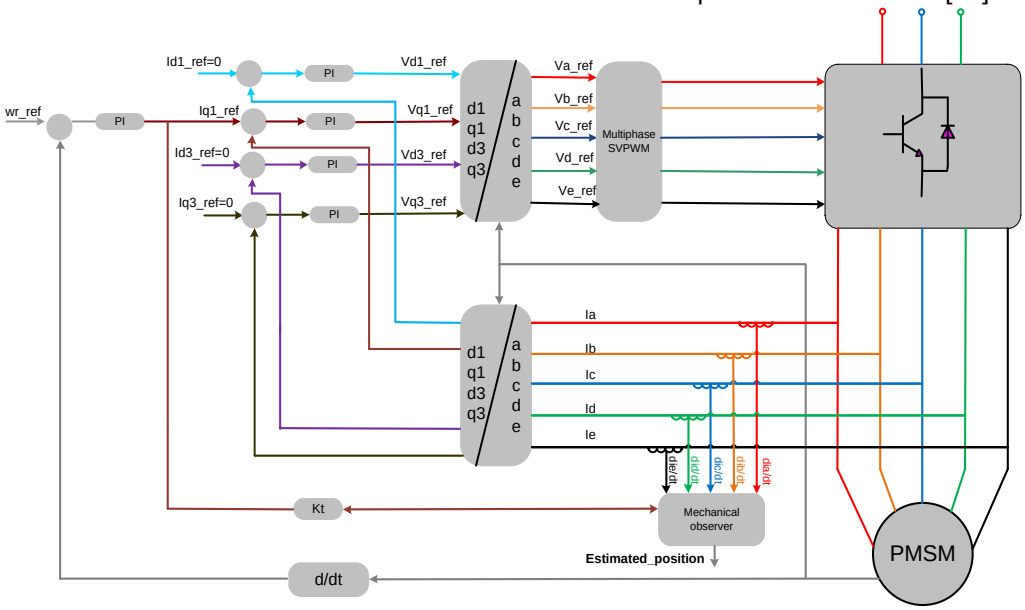

Figure 9 saliency tracking control topology for five phase drive

The results shown in figure10 demonstrate the validity of the saliency tracking algorithm. The motor was working at zero speed and at no load. At t=0.25 s a speed step change from 0 rpm to 60 rpm was applied to the system. Then at t=0.75 s a load step is applied to the system. After that between t=3 s and t=4 s a zero speed was applied to the system and finally at t=4s a speed step change from 0 rpm to 60 rpm was applied to the system The results show that the motor responded to the load and speed steps very fast and the proposed algorithm could track the saturation saliency (2*fe) both at no load at load conditions and more importantly at low and zero speeds.

3.2 Fully Sensorless Speed Control

The speed control for a five-phase PM machine drive has been implemented in simulation in the Saber modeling environment. This estimated speed $\omega_r\hat{}$ and position $\theta_r\hat{}$ are used to obtain a fully sensorless speed control as shown in figure 11.
Figure 12 demonstrate the stability of the fully sensorless system when a load disturbance where applied at low speed (50 rpm). The motor was working at 50 rpm and no load. Then a full load step is applied to the motor between t=1 s and t=3 s. between t=3 s and t=4 s the load is removed and the motor became working at no load. After that at t= 4s a speed step of -50 rpm is applied to the motor. Between t=5 s and t= 7s a negative full load step was applied. Finally at t=7s the load is removed and the motor returned to work at no load. The results shows that the system maintained the speed in all the cases.

Figure 13 shows the results of a fully sensorless speed control of a five phase PMSM motor driven by a five phase inverter at a half load condition using the algorithm presented in this paper. The motor was working in sensorless mode at speed =0.5 Hz then at time t=6 s a speed step change from 0.5 Hz to 0 rpm (till t=8 s) is applied to the system. Figure 13 shows that the motor responded to the speed step with a good transient and steady state response.

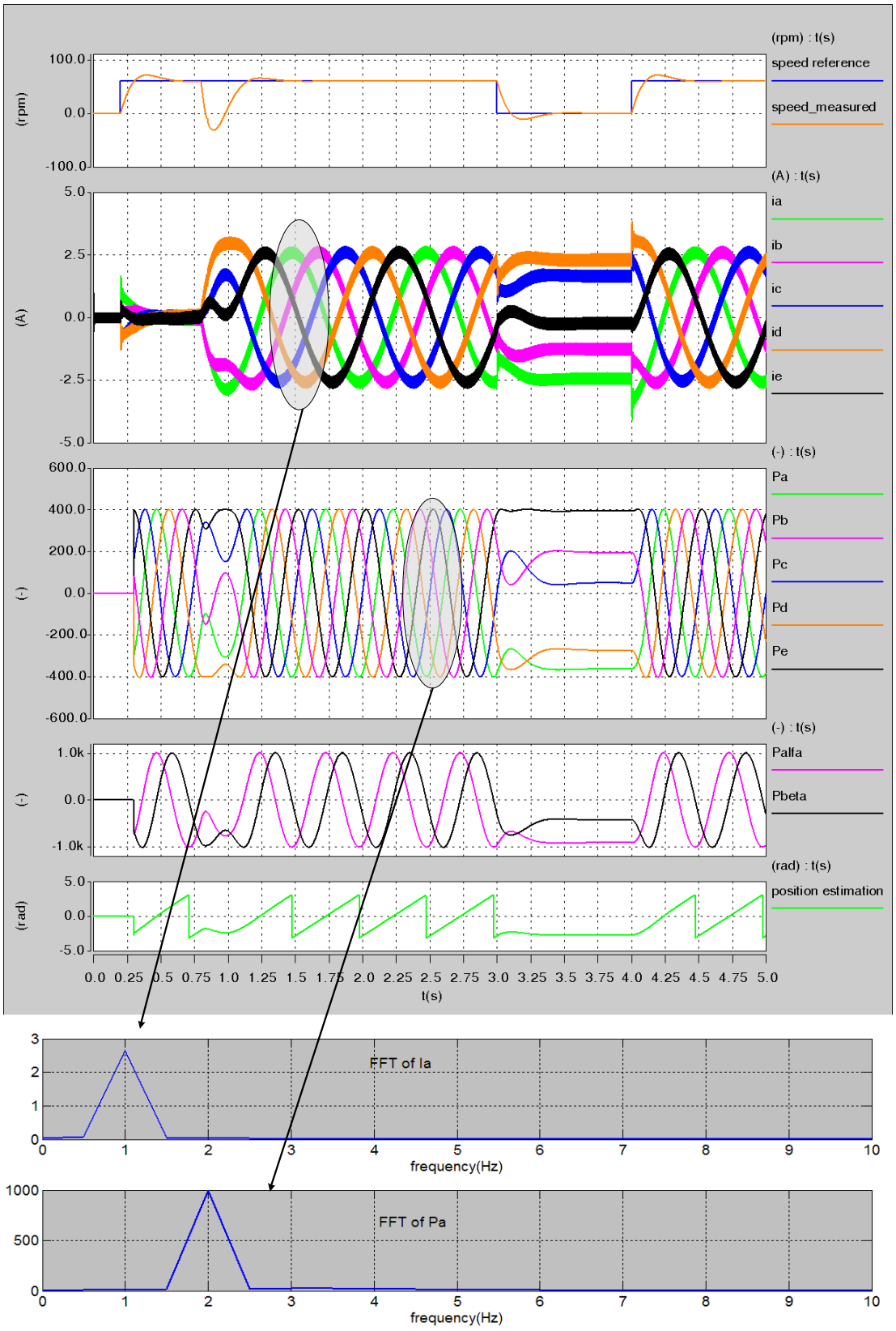

Figure 10. saliency tracking results

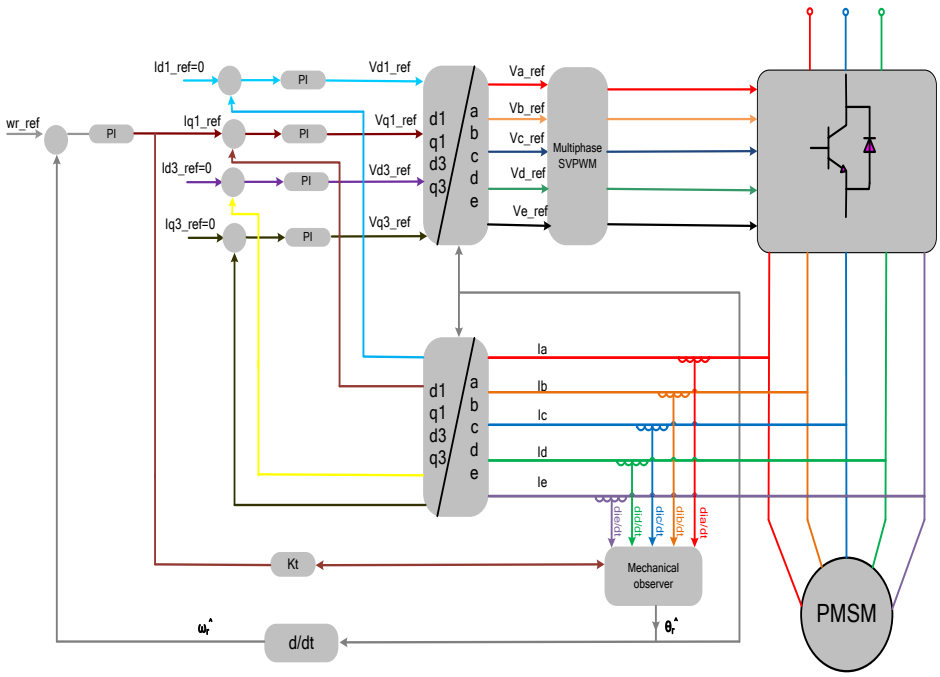

Figure11. the sensorless vector control structure for the five-phase inverter PMSM drive

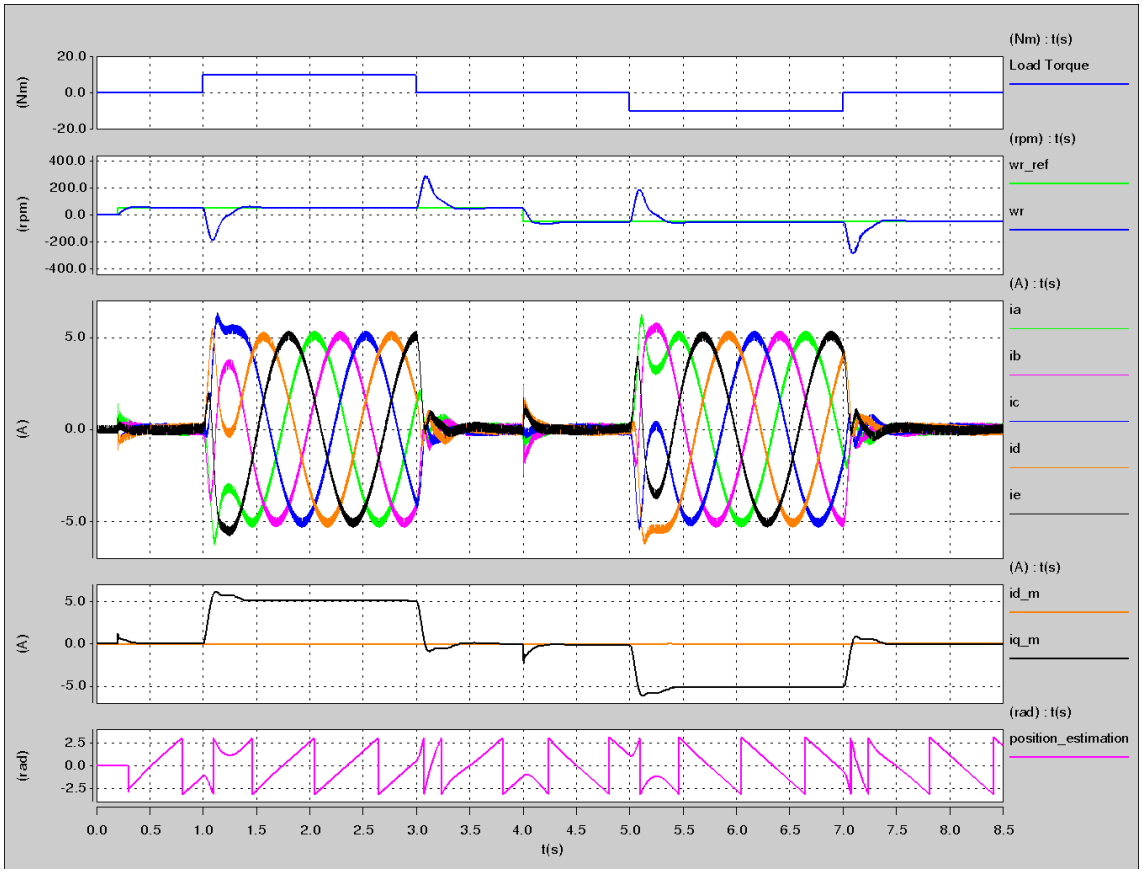

Figure 12 Fully Sensorless full load Steps.

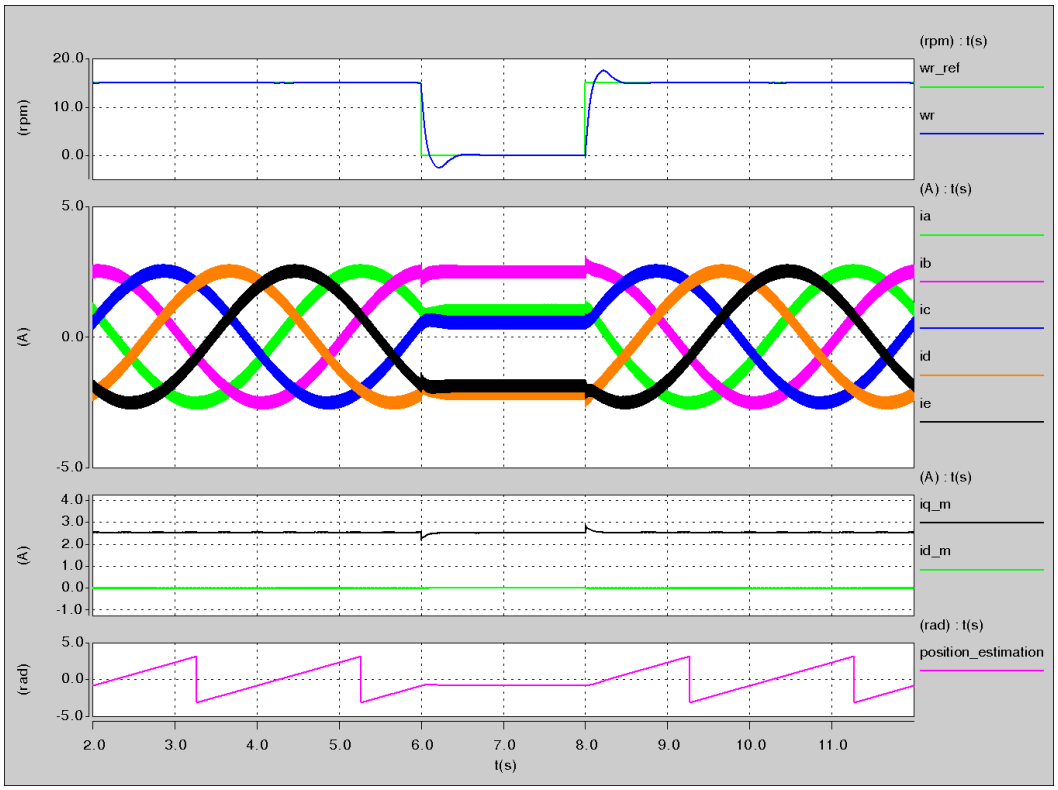

Figure 13 Fully Sensorless Speed Steps between 0.5 Hz,0 to 0.5 Hz at half load.

4. Conclusion

This paper has outlined a new scheme for tracking the saliency of motor fed by a five-leg inverter in through measuring the dynamic current response of the motor line currents due the IGBT switching actions. The proposed method includes software modification to the method proposed in[18] to track the saliency of the motor fed by three phase inverter . The new strategy can be used to track the saturation saliency in PM and the rotor slotting saliency in induction motors. The results have shown the effectiveness of the new method in increasing the safety measures in critical systems needs a continued operation.

References

[1] Villani M, Tursini M, Fabri G, Castellini L. Multi-phase fault tolerant drives for aircraft applications. In: IEEE 2010 Electrical Systems for Aircraft, Railway and Ship Propulsion Conference (ESARS); 19-21 October 2010; Bologna, Italy. New York, NY, USA: IEEE. pp. 1–6.

[2] Qingguo S, Xiaofeng Z, Fei Y, Chengsheng Z. Research on space vector PWM of five-phase three-level inverter. In: IEEE 2005 Electrical Machines and Systems conference (ICEMS); 29-29 September 2005; Nanjing, China. New York, NY, USA: IEEE. pp. 1418-1421.

[3] Ruhe S, Toliyat HA. Vector control of five-phase synchronous reluctance motor with space vector pulse width modulation (SVPWM) for minimum switching losses. In: IEEE 2002 Applied Power Electronics Conference and Exposition (APEC);10-14 March 2002; Dallas, Texas, USA. New York, NY, USA: IEEE. pp. 57-63.

[4]Abbas MA, Christen R, Jahns T.M. Six-phase voltage source inverter driven Induction motor. IEEE T Ind Appl 1984; 20: 1251-1259.

[5] Zhao X, Lipo TA. Space vector PWM control of dual three-phase induction machine using vector space decomposition. IEEE T Ind Appl 1995; 31:1177-1184.

[6] Parsa L, Toliyat HA. Multi-phase permanent magnet motor drives. In: IEEE 2003 Industry Applications Conference (IAS); 12-16 October 2003; Utah, USA. New York, NY, USA: IEEE. pp. 401-408.

[7] Xu H, Toliyat HA, Pertersen LJ. Five-phase induction motor drives with DSP-based control system. IEEE T Ind Appl 2002; 17: 524-533.

[8] Kelly JW, Strangas EG, Miller JM. Multiphase space vector pulse width modulation. IEEE T Energy Conver 2003; 18: 259-264.
[9] Xue S, Wen X, Feng Z. A novel multi-dimensional SVPWM strategy of multiphase motor drives. In: EPE 2006 Power Electronics and Motion Control Conference; 30 August- 1 September 2006; Portoroz, Slovenia. Brigitte Sneyers, Pleinlaan 2, Brussels, Belgium: EPE. pp.931-935.
[10] Pengfei W, Ping Z, Fan W, Jiawei Z, Tiecai L. Research on dual-plane vector control of five phase fault-tolerant permanent magnet machine. In: IEEE 2014 Transportation Electrification Asia-Pacific conference (ITEC Asia-Pacific); 31 August- 3 September 2014; Beijing, China. New York, NY, USA: IEEE. pp. 1-5.
[11] Minghao T, Wei H, Ming C. A novel space vector modulation strategy for a five-phase flux-switching permanent magnet motor drive system. In: IEEE 2014 Electrical Machines and Systems conference (ICEMS); 22-25 October 2014; Hangzhou, China. New York, NY, USA: IEEE. pp.1622-1628.
[12] Keng-Yuan Chen. Multiphase pulse-width modulation considering reference order for sinusoidal wave production. In: IEEE 2015 Industrial Electronics and Applications conference (ICIEA); 15-17 June 2015; New Zealand, Auckland. New York, NY, USA: IEEE. pp.1155-1160.
[13] Jansen PL, Lorenz RD. Transducerless position and velocity estimation in induction and salient AC machines. IEEE T Ind Appl 1995; 31:240–247.
[14] Jung-IkH, OhtoM, Ji-Hoon J, Seung-Ki S. Design and selection of AC machines for saliency-based sensorless control. In: IEEE 2002 Industrial Applications Conference; 13-18 October 2002; Pittsburgh, USA. NewYork, NY, USA: IEEE.pp.1155–1162.
[15] Linke M, Kennel R , Holtz J. Sensorless speed and position control of synchronous machines using alternating carrier injection. In: IEEE 2003 International Electric Machines and Drives Conference; 1-4 June 2003; Wisconsin, USA. New York, NY, USA: IEEE.pp.1211–1217.
[16] Schroedl M. Sensorless control of AC machines at low speed and standstill based on the INFORM method. In: IEEE 1996 Industry Applications Conference; 6 -10 October 1996; San Diego, USA. New York, NY, USA: IEEE. pp. 270-277.
[17] Holtz J, Juliet J. Sensorless acquisition of the rotor position angle of induction motors with arbitrary stator winding. In:IEEE 2004 Industry Applications Conference; 3-7 October 2004;Washington, USA. NewYork, NY, USA: IEEE. pp.1321-1328.
[18] Qiang G, Asher GM, Sumner M, Makys P. Position estimation of AC machines at all frequencies using only space vector PWM based excitation. In: IET 2006 International Conference on Power Electronics, Machines and Drives; 4-6 April 2006; Dublin, Ireland. Savoy Place, London, UK: IET.pp. 61-70.
[19] Z.M.S.El-Barbary. DSP Based Vector Control of Five-Phase Induction Motor Using Fuzzy Logic Control. International Journal of Power Electronics and Drive System (IJPEDS) Vol.2, No.2, June 2012, pp. 192~202
[20] Atif Iqbal, Shaikh Moinoddin*, Khaliqur Rahman. Finite State Predictive Current and Common Mode Voltage Control of a Seven-phase Voltage Source Inverter. International Journal of Power Electronics and Drive System (IJPEDS) Vol. 6, No. 3, September 2015, pp. 459~476
[21] Olivieri C, Fabri G, Tursini M. Sensorless control of five-phase brushless DC motors. In: IEEE 2010 Sensorless Control for Electrical Drives conference (SLED); 9-10 July 2010; Padova, Italy. NewYork, NY, USA: IEEE. pp.42-31.
[22] Karampuri R, Prieto J, Barrero F, Jain S. Extension of the DTC technique to multiphase induction motor drives using any odd number of phases. In: IEEE 2014 Vehicle Power and Propulsion Conference (VPPC); 27-30 October 2014; Coimbra, Portugal. NewYork, NY, USA: IEEE. pp.1-6.
[23] Parsa L, Toliyat HA. Sensorless direct torque control of five-phase interior permanent-magnet motor drives. IEEE T Ind Appl 2007; 43: 952 – 959.
[24] wubin K, Jin H, Ming K, Bingnan L. Research of sensorless control for multiphase induction motor based on high frequency injection signal technique. In: IEEE 2011 Electrical Machines and Systems conference (ICEMS); 20-23 August 2011; Beijing, China. NewYork, NY, USA: IEEE. pp.1-5.
[25] Minglei G, Ogasawara S, Takemoto M. An inductance estimation method for sensorless IPMSM drives based on multiphase SVPWM. In: IEEE 2013 Future Energy Electronics Conference (IFEEC); 3-6 November 2013; Tainan, Taiwan. NewYork, NY, USA: IEEE. pp.646-651.